JOURNAL OF SOLID STATE CHEMISTRY 116, 45–52 (1995)

Synthesis, Crystal Structure, and Electronic Structure of $InCdBr_3$

Richard Dronskowski[1]

Max-Planck-Institut für Festkörperforschung, Heisenbergstrasse 1, 70 569 Stuttgart, Germany

Received May 3, 1994; in revised form August 17, 1994; accepted August 19, 1994

Colorless crystals of diamagnetic $InCdBr_3$ are synthesized from elemental Cd in an $InBr_3$ melt. The new phase crystallizes in the orthorhombic NH_4CdCl_3 structure type (a = 944.7(2) pm, b = 410.47(8) pm, c = 1545.5(3) pm, *Pnma*, and Z = 4). Cd^{2+} is octahedrally coordinated by Br^- anions whereas the monovalent In^+ cation is located in a strongly distorted trigonal Br^- prism, tricapped by other Br^- anions. Semiempirical band structure calculations (CSC-EH-TB) show moderately strong covalent contributions to In^+–Br^- bonding, similar to those found in the binary In/Br crystal chemical system. The quality of the semiempirical calculations is compared in detail with *ab initio* band structure computations (TB-LMTO-ASA). Valence charge density plots based on the latter disprove the existence of a directed electron "*lone-pair*" *residing on monovalent* In^+.

1. INTRODUCTION

The structural richness of monovalent indium, for which various coordination polyhedra are observed, is easily demonstrated by the crystal chemistry of the binary indium bromides (1–5). Quantum mechanical bonding studies (6) indicate that the reason for this diversity lies in the importance of the filled indium 5*s* atomic orbital at the frontier bands. Any coordination polyhedron giving sufficient space for In^+, aside from repelling anion–anion interactions, is equally appropriate and leads to similar bonding energies.

After having completed both structural and electronic studies on the new phases $InFeBr_3$ and $InMnBr_3$ (crystallizing in the NH_4CdCl_3 structure type) (7), the synthesis of $InCdBr_3$ should serve two purposes. First, significant contributions to the observed structural distortions (equally present in the isotypic Fe and Mn compounds) could be solely attributed to the In^+ since Cd^{2+}, unlike Fe^{2+} or Mn^{2+}, has a filled *d* shell. Second, since $InCdBr_3$ was proposed to be diamagnetic, the compound should serve as an ideal test case for a detailed comparison between charge-self-consistent semiempirical band structure calculations (*limited* to the non-spin-polarized case) and corresponding *ab initio* computations (*performed* in the non-spin-polarized mode). In the following, we will comment on the synthesis, crystal structure, and electronic structure of the new phase $InCdBr_3$.

2. EXPERIMENTS AND THEORY

2.1. Synthesis

Quantitative yields of $InCdBr_3$ were synthesized by melting equimolar amounts of freshly prepared $InBr_3$ and metallic cadmium powder (Merck, p.a.) within evacuated glass ampoules at 450°C for 5 days. The preparation of $InBr_3$ followed the aqueous solution route (8), thereafter it was purified by repeated sublimation. The melt was cooled to 100°C at a rate of 2°C/hr, and then to room temperature at 20°C/hr. The colorless transparent needles of $InCdBr_3$ are extremely sensitive with respect to humidity and must be protected under argon.

2.2. Crystal Structure Analysis

The presence of the orthorhombic crystal class was apparent from an X-ray Guinier diagram, showing the following characteristic reflections (*d* value in pm (*hkl*) relative intensity): 772.8 (002) 10, 598.1 (102) 13, 452.3 (103) 15, 365.8 (111) 17, 348.2 (203) 11, 304.0 (113) 31, 303.8 (211) 99, 299.1 (204) 34, 293.8 (105) 52, 291.6 (302) 21, 287.6 (212) 100, 248.5 (106) 12, 246.9 (015) 37, 244.1 (304) 10, 214.7 (403) 19, 212.6 (116) 11, 209.8 (314) 39, 205.2 (020) 41, 204.7 (410) 11, 200.0 (207) 11, 190.5 (117) 30, 190.2 (413) 13, 169.2 (224) 14, 168.2 (125) 22, 160.3 (416) 10, 150.8 (309) 18, 148.4 (423) 13, 131.0 (231) 10, 129.6 (232) 12, 123.3 (622) 11, 121.5 (329) 24, 114.2 (01, 13) 10.

The orthorhombic unit cell was confirmed from axes photographs of a single crystal mounted on a four-circle diffractometer. After correcting semiempirically for absorption (9), the systematic absences led to the expected space groups $Pna2_1$ and *Pnma*. The structure refinement in *Pnma* (SHELXL-93) (10) converged easily after having started with the parameters of NH_4CdCl_3 and using scattering factors of the neutral atoms (11). The R_1 residual

[1] E-mail: drons@simix.mpi-stuttgart.mpg.de.

0022-4596/95 $6.00

TABLE 1
Crystallographic Data for $InCdBr_3$

Formula, molar mass	$InCdBr_3$, 466.94 g/mole
Lattice constants	a = 944.7(2) pm, b = 410.47(8) pm, c = 1545.5(3) pm Stoe powder diffractometer, 44 reflections ($10° < 2\theta < 85°$)
Molar volume	90.24(3) cm^3/mole
Space group, formula units	$Pnma$–D_{2h}^{16} (No. 62), 4
X-ray density, $F(000)$	5.175 g/cm^3; 720
Absorption coefficient	27.24 mm^{-1}
Crystal dimensions	0.110 × 0.055 × 0.035 mm^3
Instrument	Enraf–Nonius CAD4 four circle diffractometer, Mo$K\alpha$ radiation, graphite monochromator, scintillation counter
Scan range, scan type	$5° < 2\theta < 60°$; ω-θ scan
Scan speed	Variable, prescan-dependent
Temperature	293 K
Number of reflections	1891, 978 unique
Octants	$0 \le h \le 13$, $-5 \le k \le 5$, $0 \le l \le 21$
Absorption correction	ψ scan with 4 reflections, Pseudoellipsoid
Min, max transmission	0.046, 0.097
R_{int}; R_σ	0.103, 0.131
Structure solution	Parameters of NH_4CdCl_3
Structure refinement	Least-squares method, full matrix
No. of intensities, variables, restraints	966, 32, 0
Weighting scheme	$w = 1/[\sigma^2(F_o^2) \times (0.0140 \times P)^2]$, $P = (\max(F_o^2, 0) + 2 \times F_c^2)/3$
Min, max, mean residual electron density	−1.38, 1.58, 0.01(33) e/Å^3
Extinction correction	x = 0.0008(1)
R_1 ($F_o > 4\sigma(F_o)$)	0.055
wR_2, goodness of fit (all data)	0.084, 0.935

(12) dropped to 0.055 when extinction effects were included in the refinement. An alternative refinement in the acentric space group $Pna2_1$ was less successful; the wR_2 residual was larger by more than 0.06 and the standard deviations for the positional parameters increased by more than one order of magnitude.

Despite the fact that the components of the anisotropic displacement factors are well behaved for all the atoms, it is worthwhile mentioning that the isotropic displacement factor of In is significantly larger than those of the four other atoms inside the asymmetric unit. This effect has already been noted (7) in the structures of $InFeBr_3$ and $InMnBr_3$ and it is not due to a suboccupation of the indium site since its occupation factor is 1.006(5). Electronic mechanisms are responsible for this phenomenon (13).

The final difference Fourier map is flat and the strongest residual peak is about 116 pm from the Br(3) atom. Table 1 shows all relevant data of the structure analysis while Table 2 contains positional and isotropic displacement parameters. Anisotropic displacement parameters are given in Table 3. Table 4 lists all important interatomic distances (14).

2.3. Magnetic Measurement

The magnetic susceptibility of a 119-mg sample of crystalline $InCdBr_3$ was measured by use of a Quantum Design MPMS 5.5 Squid susceptometer within a temperature range of 5–300 K at a field strength of 1 kG. As expected, $InCdBr_3$ is diamagnetic with a susceptibility of about -1.1×10^{-4} emu/mole.

TABLE 2
Positional Parameters (All Atoms on Special Position 4c, $y \equiv 1/4$) and Isotropic Displacement Parameters[a] (pm^2) for $InCdBr_3$ (Standard Deviations in Parentheses)

Atom	x	z	U_{eq}
In	0.4393(2)	0.6770(1)	533(5)
Cd	0.1675(2)	0.4429(1)	314(4)
Br(1)	0.6665(2)	0.4939(1)	298(5)
Br(2)	0.2873(2)	0.2867(1)	367(5)
Br(3)	0.0245(2)	0.6043(1)	275(5)

[a] U_{eq} is a third of the trace of the orthogonalized U_{ij} tensor.

TABLE 3
Anisotropic Displacement Parameters[a] (pm^2) for $InCdBr_3$ (Standard Deviations in Parentheses); $U_{23} \equiv U_{12} \equiv 0$

Atom	U_{11}	U_{22}	U_{33}	U_{13}
In	637(12)	477(11)	486(10)	−35(10)
Cd	337(9)	289(7)	316(7)	25(7)
Br(1)	244(10)	290(10)	360(10)	−16(9)
Br(2)	411(13)	364(12)	325(11)	83(10)
Br(3)	273(10)	299(11)	254(9)	18(8)

[a] The components U_{ij} refer to a displacement factor of the form $\exp\{-2\pi^2(U_{11}h^2a^{*2} + \cdots + 2U_{23}klb^*c^*)\}$.

2.4. Thermoanalytical Investigation

A differential thermoanalytical analysis on a 500-mg sample of $InCdBr_3$ was performed using a Heraeus DTA 500 instrument. The sample was sealed in an evacuated quartz capillary. A temperature range of 25–400°C was scanned with a scan speed of 5°C/min. No other thermal effect was observed except the compound's melting point at 348°C.

2.5. Electronic Structure Investigation

The electronic structure calculations on $InCdBr_3$ were performed at two different levels of sophistication. Semiempirical tight-binding calculations helped in the analysis of the chemical bonding, whereas first principles computations led to the generation of charge density plots. As stated above, a detailed numerical comparison between the two approaches was attempted in order to estimate the quality of the semiempirical method. All computations were carried out either on a DECstation 5000/133 or on an IBM RS 6000/520 machine, running under the UNIX operating system.

2.5.1. Semiempirical calculations. The semiempirical calculations on $InCdBr_3$ were started from tabulated Coulomb integrals using the simplified one-electron Hamiltonian of charge-self-consistent (15) extended Hückel theory (16). Within the iterative process towards self-consistency, the amount of electron correlation was corrected up to first order by varying all atomic Coulomb integrals dependent on atomic charge and electronic configuration. The charge dependence of the valence orbitals' ionization potentials was approximated by a quadratic power series. The explicit charge iteration parameters for In and Br were the same as in two preceding studies (6, 7) whereas those of the cadmium atom were taken from the work of Munita and Letelier (17).

Slater-type orbital exponents for In and Br were based on numerical atomic wavefunctions that had been given by Pyykkö and Lohr (18). Exponents for Cd were taken from the work of Fitzpatrick and Murphy (Herman–Skillman fits) (19). A minimal set of Slater functions for In (5*s*, 5*p*), Br (4*s*, 4*p*), and Cd (5*s*, 5*p*, 4*d*) was used throughout. The amount of counterintuitive orbital mixing within the minimal basis set was minimized by computing the off-site Hamiltonian matrix elements as defined in the weighted WH formula (20). The eigenvalue problem was solved in reciprocal space at 42 k points within the irreducible wedge of the Brillouin zone, using a modified EHMACC code (21).

2.5.2. First-principles calculations. Electronic structure calculations of *ab initio* quality were performed using LMTO (linear muffin-tin orbital) theory (22–25), a fast linearized form of the KKR method (26, 27). The method accounts for the potential from all the electrons and is applicable to materials composed of atoms from any part of the periodic table. Its almost minimal, unfixed basis sets adjust dynamically to the respective potentials. In the interstitial regions with flat potentials, the wave func-

TABLE 4
Interatomic Distances (pm) in $InCdBr_3$ (Standard Deviations in Parentheses)

In–Br(2*d*)	334.6(2)	In–In(*b*)	410.47(8)
–Br(2*c*)	334.6(2)	–In(*a*)	410.47(8)
–Br(2*i*)	341.6(2)	–Cd	443.6(2)
–Br(2*j*)	341.6(2)		
–Br(3*l*)	347.5(2)		
–Br(1*c*)	349.2(2)		
–Br(1*d*)	349.2(2)		
–Br(1)	355.2(3)		
–Br(3)	407.7(3)		
Cd–Br(2)	266.7(2)	Cd–Cd(*b*)	410.47(8)
–Br(1*d*)	276.1(2)	–Cd(*a*)	410.47(8)
–Br(1*c*)	276.1(2)	–Cd(*g*)	416.4(3)
–Br(3*g*)	283.4(2)	–Cd(*h*)	416.4(3)
–Br(3*h*)	283.4(2)		
–Br(3)	283.6(2)		
Br(1)–Br(1*c*)	376.1(3)	Br(2)–Br(3*e*)	391.5(2)
–Br(1*d*)	376.1(3)	–Br(3*f*)	391.5(2)
–Br(3*k*)	378.8(3)	–Br(3*g*)	396.6(2)
–Br(3*d*)	387.7(2)	–Br(3*h*)	396.6(2)
–Br(3*c*)	387.7(2)	–Br(2*b*)	410.47(8)
–Br(2*d*)	398.7(2)	–Br(2*a*)	410.47(8)
–Br(2*c*)	398.7(2)		
–Br(1*b*)	410.47(8)		
–Br(1*a*)	410.47(8)		
Br(3)–Br(3*g*)	384.9(3)		
–Br(3*h*)	384.9(3)		
–Br(3*a*)	410.47(8)		
–Br(3*b*)	410.47(8)		

Note. Symmetry coding (including lattice translations): (*a*) $x, y - 1, z$; (*b*) $x, y + 1, z$; (*c*) $-x + 1, -y, -z + 1$; (*d*) $-x + 1, -y + 1, -z + 1$; (*e*) $-x + 1/2, -y, z - 1/2$; (*f*) $-x + 1/2, -y + 1, z - 1/2$; (*g*) $-x, -y, -z + 1$; (*h*) $-x, -y + 1, -z + 1$; (*i*) $-x + 1/2, -y, z + 1/2$; (*j*) $-x + 1/2, -y + 1, z + 1/2$; (*k*) $x + 1, y, z$; (*l*) $x + 1/2, y, -z + 3/2$.

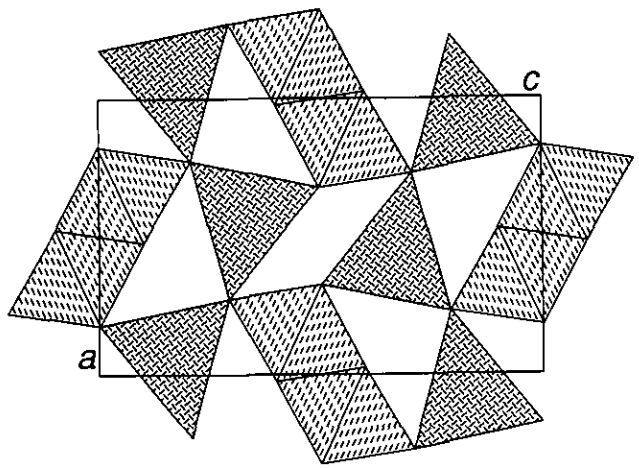

FIG. 1. Polyhedral projection of the $InCdBr_3$ crystal structure along the *b* axis. The In^+ ions are located inside trigonal Br^- prisms (herringbone pattern), whereas the Cd^{2+} ions are found in vertice-sharing Br^- octahedra (dashed lines). See text for more details.

tions of the valence electrons are expanded into Hankel envelope functions whereas in the core-like regions one seeks numerical solutions of the radial Schrödinger equation.

For $InCdBr_3$, the electronic energy was computed with the help of density-functional theory, replacing the many-particle problem by the self-consistent solution of the Kohn–Sham equations (28, 29), taking the von Barth and Hedin parametrization (30). The non-spin-polarized Hamiltonian corresponded to a scalar relativistic calculation of the electronic structure. The integration in *k* space was performed with the help of an improved (31) tetrahedron method (32) using 16 inequivalent *k* points and 123 different tetrahedra. A minimal basis set of short-range atom-centered TB-LMTO's was used (33), which has one *s*, three *p*, and five *d* orbitals on each of the atoms. Indium and bromine *d* orbitals were included using a downfolding technique. Starting from atomic Hartree potentials, the structure was iterated by use of the atomic-spheres approximation (ASA), employing muffin-tin spheres expanded to overlapping and volume filling spheres (including a combined correction term). After having reached self-consistency, charge density plots were generated upon switching to full-potential LMTO mode, dropping any shape approximations for the charge density. The program used corresponds to the TB-LMTO 4.4 code (34).

3. RESULTS AND DISCUSSION

3.1. Description of the Crystal Structure

The crystal structure of $InCdBr_3$, depicted as a projection in Fig. 1, belongs to the NH_4CdCl_3 type. The Cd^{2+} ion is surrounded by six Br^- ions to form a slightly distorted octahedron. The average Cd^{2+}–Br^- bond length is 278.2 pm and individual deviations from this value are smaller than 12 pm. Such an octahedron is laterally connected with four other octahedra by sharing five of its vertices, resulting in a double chain of octahedra running parallel to the short *b* axis.

The univalent indium ion rests in a strongly distorted trigonal prism of which a thermal ellipsoid plot is given in Fig. 2. The prism's three rectangular faces are capped by additional bromine ions from inside the unit cell while the top and the bottom faces are covered by indium ions of neighboring unit cells. This results in an indium–indium distance of 410.47 pm.

Above grouping of the coordinating Br^- into inner- and outer-prism ions is admittedly idealized. First, the three "inner" In^+–Br^- bond lengths (each occurring twice) cover the range 335–349 pm. Second, at least one of the "outer" face-capping Br^- ions (Br(31) in Fig. 2) has an equally short In^+–Br^- bond distance, namely 348 pm. Finally, there is a large variance in the In^+–Br^- bond lengths of the face-capping Br^- ions. Here one observes distances of 348, 355, and 408 pm so that there is one face-capping ligand (Br(3) in Fig. 2) which is about 16% further from In^+ compared to Br(1) and Br(31).

The present coordination is identical with the one found in $InFeBr_3$ and $InMnBr_3$. It could be shown, however, that there is no directed electron "lone-pair" acting on

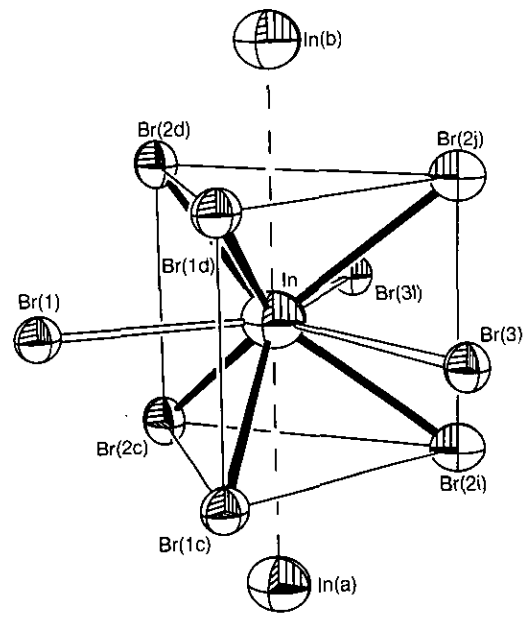

FIG. 2. Perspective view of the In^+ coordination by Br^- ions in $InCdBr_3$. The ellipsoids enclose 70% of the electrons' spatial probability. In^+–Br^- bonds are given as solid (Br^- ions inside trigonal prism) and open lines (face-capping Br^- ions), whereas the shortest In^+–In^+ contacts are drawn with broken lines. The edges of the trigonal prism are emphasized by thin lines.

In^+, and the strong distortion in the Br(1)–Br(3)–Br(3l) plane can only be due to optimized covalency within the trigonal prism (7). The popularity of this electron lone-pair concept within classic crystal chemistry is questionable and we will touch on its significance in the two following sections.

3.2. Structural Comparison

In order to empirically study the relationship between the local electronic structure of In^+ and the actual crystal structure, a comparison of $InCdBr_3$ with isotypic $RbCdBr_3$ seems to be most appropriate (35). Concerning their Cd/Br partial metrics, both structures are practically identical. For example, the average Cd^{2+}–Br^- distance in $RbCdBr_3$ is 278.6 pm, equivalent within two standard deviations (0.2 pm) to the value of $InCdBr_3$.

A small difference between the two structures arises from the difference in ionic radii of In^+ and Rb^+, and one would expect an increase in molar volume of about 2.54 cm^3/mole upon going from $InCdBr_3$ to $RbCdBr_3$, provided that those ionic radii are approximately additive (36). Based on Biltz's classic compilation (37) of atomic (ionic) volume increments, the increase should be 4 cm^3/mole. Indeed, $RbCdBr_3$ is larger by 2.95 cm^3/mole than $InCdBr_3$, simply due to the lengthened Rb^+–Br^- bond distances (average 355.5 pm) compared to the mean In^+–Br^- bond length (351.2 pm). The In^+–Br^- bond distances in $InCdBr_3$ are well adjusted to give a reasonable bond valence sum for In. According to the empirical one-parameter formula of Brown and Altermatt (38), the bond valence sum equals +1.02 using the recently evaluated optimum single bond distance r_0 of 266.7 pm (6).

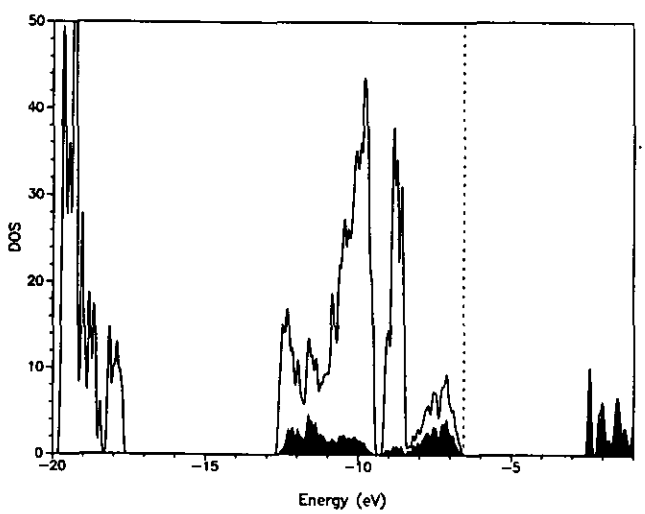

FIG. 3. CSC-EH-TB semiempirical density-of-states (DOS) of $InCdBr_3$ with In contributions emphasized in black. The energy range covers 19 eV.

TABLE 5

Semiempirical Slater Orbital Exponents ζ, Charge-Iterated Exchange Integrals H_{ii}, *ab Initio* Band Centers C, and LMTO Sphere Radii[a] r_{ws} for $InCdBr_3$

Atom	Orbital	ζ	H_{ii} (eV)	C (eV)	r_{WS} (pm)
In	5*s*	1.934	−10.593	−8.693	202.1
	5*p*	1.456	−5.824	−0.533	
	5*d*	—	—	+18.129	
Cd	5*s*	1.734	−11.028	−9.042	154.0
	5*p*	1.219	−6.298	−3.657	
	4*d*[b]		−19.344	−12.547	
Br(1)	4*s*	2.588	−22.654	−19.965	157.7
	4*p*	2.131	−9.979	−6.670	
	4*d*	—	—	+16.563	
Br(2)	4*s*	2.588	−22.590	−20.444	153.1
	4*p*	2.131	−9.868	−6.838	
	4*d*	—	—	+16.930	
Br(3)	4*s*	2.588	−22.819	−20.132	162.5
	4*p*	2.131	−10.263	−7.141	
	4*d*	—	—	+15.280	

[a] In the *ab initio* calculations, an additional 52 "empty spheres" (atomic wave functions without nuclei) per cell with sphere radii of 128.0–63.1 pm were introduced in order to decrease interatomic overlap and to improve variational freedom.

[b] In the semiempirical calculations, Cd *d* orbitals were approximated by double-zeta functions with exponents $\zeta_1 = 4.094$, $\zeta_2 = 1.640$ and weighting coefficients $c_1 = 0.824$ and $c_2 = 0.325$.

Most importantly, the large variance in In^+–Br^- bond lengths observed in the geometrical plane spread out by the face-capping bromine ions is equally present (although slightly less pronounced) in $RbCdBr_3$, the distances being 359, 363, and 397 pm. It is obvious that an electron lone-pair hypothesis is fully unsatisfactory for the Rb^+ ion, having a noble gas electron configuration. This hypothesis will be shown to be equally unreasonable for In^+.

3.3. Electronic Structure

3.3.1. Comparison between CSC-EH-TB and TB-LMTO-ASA Theory. Figure 3 shows the semiempirical total and local (In) density-of-states of $InCdBr_3$. The main features are easy to explain: Indium 5*s* wave functions contribute mainly to those levels which are dominated by the bromine 4*p* orbitals; this is the region above −13 eV going up to the Fermi level (dashed line). Indium 5*p* orbitals mix in with a significantly smaller amount, at around −10.5 eV. The virtual levels above −3 eV, however, are practically pure In 5*p* bands. The region below −17 eV may be described as semicore bands that are almost completely cadmium 4*d* in character.

To get an estimate of the quality of this semiempirical result concerning the *orderings* of the bands, a look at Table 5 reveals the appropriate comparison between charge-iterated H_{ii} values and *ab initio* band centers C.

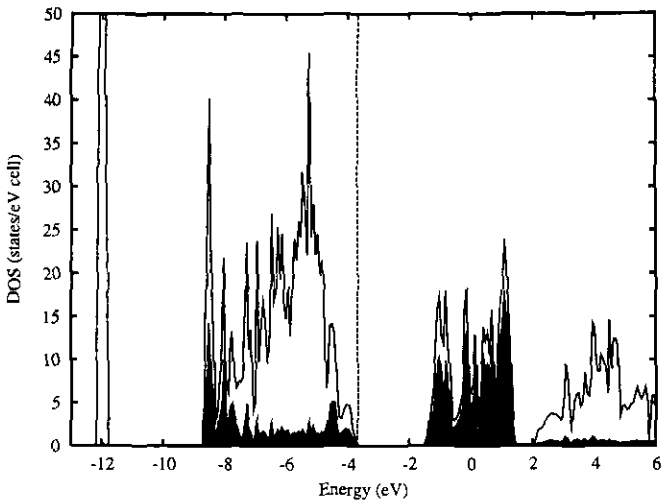

FIG. 4. TB-LMTO-ASA *ab initio* density-of-states (DOS) of $InCdBr_3$ with In contributions emphasized in black. The energy range covers 19 eV.

Neglecting the difference in zeros of both scales (39), there is an almost one-to-one correspondence between them (40). For example, the ordering in energy going down the bands starting at the Fermi level (Br 4*p*, In 5*s*, Cd 5*s*, Cd 4*d*, Br 4*s*) is the same. Relative energy differences such as In 5*s*–Cd 5*s* are nearly equivalent (semiempirical: 0.44 eV, *ab initio*: 0.35 eV) or still similar like Br 4*p*–In 5*s* (semiempirical: 0.56 eV, *ab initio*: 1.81 eV). The smaller energy difference for the latter reflects the slight overestimation of covalency in the semiempirical calculation.

Stronger differences between both methods are easier to visualize from the *ab initio* density-of-states in Fig. 4, to be compared with the preceding DOS in Fig. 3. There are two main failures in the semiempirical description: First, the low-lying Cd 4*d* semicore levels are very sharp and nearly dispersion-free in the *ab initio* calculation. The semiempirical method, however, overestimates the dispersion by a good amount, possibly because the Cd 4*d* basis functions are too diffuse. Second, the inner gap between these Cd semicore levels and the Br 4*p* dominated bands is only about 3 electron volts (*ab initio*) and not close to 5 eV (semiempirical), a failure that must be due to insufficient parametrization.

It is not clear at present whether the band gap between filled and the closest virtual levels (also mainly indium 4*p* in the *ab initio* DOS) is more accurate in the *ab initio* calculation (2.1 eV) or in the semiempirical one (4.0 eV). The first is known to underestimate band gaps whereas the latter typically overestimates them. The shapes of the Br 4*p* bonding regions are similar (but still different) in both calculations and the widths of the blocks are also similar (*ab initio*: 5 eV, semiempirical: 6 eV). In short, taking into account the energy ordering of the frontier bands and neglecting the improper description of the semicore levels, one may expect the semiempirical calculation to give a very meaningful description of the chemical bonding. Before switching to it, Fig. 5 gives access to the *ab initio* bands that were used to generate the preceding *ab initio* DOS. Only here one can recognize that there are four levels with high dispersion just below the Fermi level. They arise because of the presence of the 5*s* atomic orbitals on the four symmetry-equivalent indium atoms contained in the primitive unit cell. The existence of these filled 5*s* frontier bands has already been noted in a previous publication, and the consequences concerning acid–base behavior were highlighted (6).

3.3.2. Analysis of chemical bonding. The crystal orbital overlap population (COOP) plot in Fig. 6 reflects the bonding of In^+ to its nine nearest Br^- neighbors. In a manner similar to In^+–Br^- bonding inside InBr and $InBr_2$, there are visible both In^+–Br^- bonding levels below about −9.5 eV as well as strongly *antibonding* contributions above that energy. The latter effect results from an out-of-phase combination between indium 5*s* and bromine 4*p* orbitals, a common phenomenon of all known In^+–Br^- interactions within crystalline solids (6). Such a bonding pattern, however, is very atypical for most other crystal structures. More quantitatively (summing up all these interactions to the Fermi energy), one yields an integrated COOP (ICOOP) value of 0.060, which is normal only for In^+–Br^- bonding (41).

The short contacts between In^+ ions of neighboring unit cells (see the broken lines in Fig. 2) lead to the question of possible covalent bonding interactions. There are only

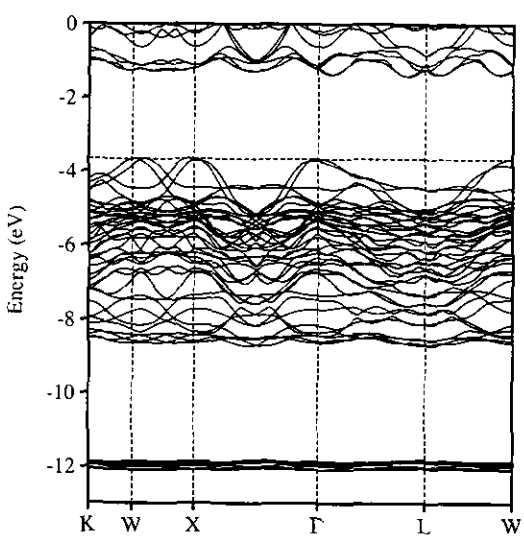

FIG. 5. TB-LMTO-ASA *ab initio* band structure of $InCdBr_3$. The special points refer to a Brillouin zone of a primitive orthorhombic unit cell.

very small bonding effects arising from the diffuse indium 5*s* atomic orbitals spilling over into the neighboring unit cells. The integrated COOP value is 0.067, about 30% smaller (on the average) than the corresponding interactions in isotypic $InFeBr_3$ and $InMnBr_3$, a result of the 14-pm-widened *b* axis of $InCdBr_3$.

Switching back to the *ab initio* calculations, Fig. 7 shows a computed valence charge density plot after having reached self-consistency. Depicted is the lattice plane spread out by the bromine atoms Br(1), Br(3), and Br(31) of Fig. 2, this shows the three face-capping bromine ions around the trigonal prism. Analogous to a previous study (7), two observations can be made: Upon comparing the indium ion with the cadmium and bromine ions, there are surprisingly large differences in the charge densities' drop-off so that the electron density around In^+ is significantly more diffuse than any other one, very likely due to a soft crystal potential at the indium site.

Even more important, there is no distortion visible with respect to the indium ion's electron density and the In–Br(3) connecting vector, this is the direction in which one might think that a so-called directed electron lone-pair might point. Also, in agreement with the structural comparison of $InCdBr_3$ and the isotypic rubidium compound, the electron density (an observable quantity) does not support a directed electron lone-pair hypothesis but clearly contradicts it. It is more reasonable to talk of an inert, nondirectional (5*s*) electron pair centered on In^+.

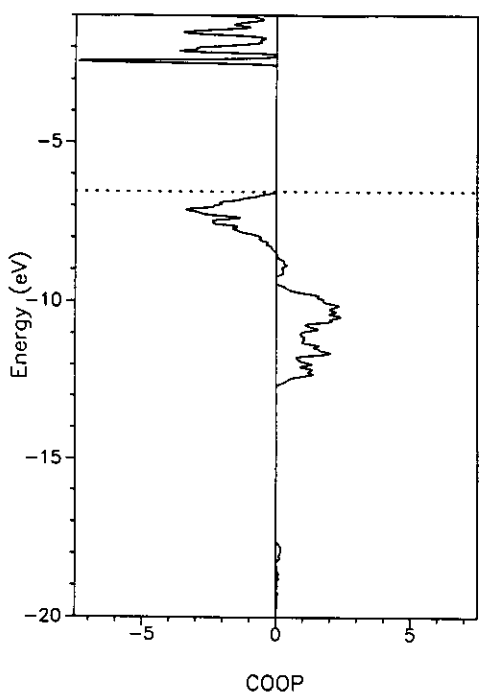

FIG. 6. Crystal orbital overlap population (COOP) of the In^+–Br^- bonding (nine nearest bonds) in $InCdBr_3$.

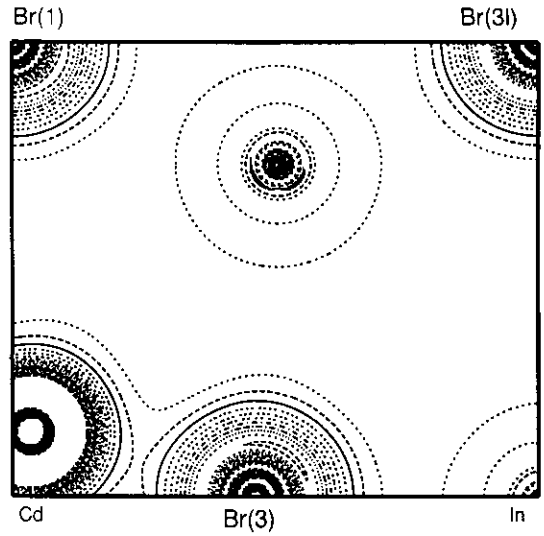

FIG. 7. Computed charge density inside $InCdBr_3$ from first principles. The observable is given in 20 equidistant steps between 0 and 0.35 e/a_0^3 (a_0 is the Bohr radius which is about 53 pm). The outermost "ring" around the indium atom (center) is 0.0175 e/a_0^3.

In other words, any distortion of the bromine coordination around indium can only be due to the optimization of additional covalent In^+–Br^- bonding inside the prism in addition to the electrostatic interaction.

ACKNOWLEDGMENTS

The author thanks Prof. Dr. Arndt Simon for his steady and generous support. Also, the author gratefully acknowledges the careful X-ray data collection by Dr. Horst Borrmann, the susceptibility measurements by Eva Brücher and Dr. Reinhard K. Kremer, help with the powder and thermoanalytical investigations by Friedrich Kögel and Willi Röthenbach, and preparative assistance by Michael Baitinger. Expert help concerning different UNIX operating environments by Armin Schuhmacher and Dr. Armin Burkhardt is gratefully acknowledged, as are some useful hints concerning LMTO theory by Dr. Ove Jepsen and Dr. Georges Krier. Additional thanks are expressed to the Fonds der Chemischen Industrie for financial support.

REFERENCES

1. T. Staffel and G. Meyer, *Z. Anorg. Allg. Chem.* **552,** 113 (1987).
2. T. Staffel and G. Meyer, *Z. Anorg. Allg. Chem.* **563,** 27 (1988).
3. R. E. Marsh and G. Meyer, *Z. Anorg. Allg. Chem.* **582,** 128 (1990).
4. H. Bärnighausen, *Z. Kristallogr.* **186,** 16 (1989).
5. H. P. Beck, *Z. Naturforsch. B* **42,** 251 (1987).
6. R. Dronskowski, *Inorg. Chem.* **33,** 6201 (1994).
7. R. Dronskowski, *Inorg. Chem.* **33,** 5927 (1994).
8. F. Ensslin and H. Dreyer, *Z. Anorg. Allg. Chem.* **249,** 119 (1942).
9. A. C. T. North, D. C. Phillips, and F. S. Mathews, *Acta Crystallogr. Sect. A* **24,** 351 (1968).
10. G. M. Sheldrick, in preparation.
11. "International Tables for Crystallography, Volume C" (A. J. C. Wilson, Ed.). Kluwer Academic, Dordrecht, 1992.
12. R_1 is only for comparison with conventional structure factor *F* refinements. Note that SHELXL-93 refines against F^2 in order to

minimize the so-called wR_2 residual. The latter is indeed based on F^2 and is statistically about twice as large as those based on F. The definitions are $wR_2 = \sqrt{\Sigma[w(F_o^2 - F_c^2)^2]/\Sigma[w(F_o^2)^2]}$; $R_1 = \Sigma||F_o| - |F_c||/\Sigma(F_o)$

13. R. Dronskowski and U. Schönberger, in preparation.
14. A list of the observed and calculated structure factors may be obtained from the Fachinformationszentrum Karlsruhe, D-76 344 Eggenstein-Leopoldshafen, on quoting the depository number CSD-58439, the author's name, and the journal citation.
15. S. P. McGlynn, L. G. Vanquickenborne, M. Kinoshita, and D. G. Carroll, "Introduction to Applied Quantum Chemistry." Holt, Rinehart & Winston, New York, 1972.
16. R. Hoffmann, *J. Chem. Phys.* **39,** 1397 (1963).
17. R. Munita and J. R. Letelier, *Theor. Chim. Acta Berlin* **58,** 167 (1981).
18. P. Pyykkö and L. L. Lohr, Jr., *Inorg. Chem.* **20,** 1950 (1981).
19. N. J. Fitzpatrick and G. H. Murphy, *Inorg. Chim. Acta* **87,** 41 (1984); **111,** 139 (1986).
20. J. H. Ammeter, H.-B. Bürgi, J. C. Thibeault, and R. Hoffmann, *J. Am. Chem. Soc.* **100,** 3686 (1978).
21. M.-H. Whangbo, M. Evain, T. Hughbanks, M. Kertesz, S. Wijeyesekera, C. Wilker, C. Zheng, and R. Hoffmann, "QCPE program EHMACC."
22. O. K. Andersen, *Phys. Rev. B* **12,** 3060 (1975).
23. O. K. Andersen, O. Jepsen, and D. Glötzel, *in* "Highlights of Condensed-Matter Theory" (F. Bassani, *et al.*, Eds.). North-Holland, New York, 1985.
24. H. L. Skriver, "The LMTO Method." Springer, Berlin/Heidelberg/New York, 1984.
25. O. K. Andersen, O. Jepsen, and M. Sob, *in* "Electronic Band Structure and its Applications" (M. Yussouf, Ed.). Springer, Berlin/Heidelberg/New York, 1986.
26. J. Korringa, *Physica* **13,** 392 (1947).
27. W. Kohn and N. Rostoker, *Phys. Rev.* **94,** 1111 (1954).
28. P. Hohenberg and W. Kohn, *Phys. Rev. B* **136,** 864 (1964).
29. W. Kohn and L. J. Sham, *Phys. Rev. A* **140,** 1133 (1965).
30. U. von Barth and L. Hedin, *J. Phys. C* **5,** 1629 (1972).
31. P. Blöchl, Ph.D. Thesis, Universität Stuttgart, FRG, 1989.
32. O. Jepsen and O. K. Andersen, *Solid State Commun.* **9,** 1763 (1971).
33. O. K. Andersen and O. Jepsen, *Phys. Rev. Lett.* **53,** 2571 (1984).
34. M. van Schilfgaarde, T. A. Paxton, O. Jepsen, and O. K. Andersen, "TB-LMTO 4.4 Program"
35. M. Natarajan Iyer, R. Faggiani, and I. D. Brown, *Acta Crystallogr. Sect. B* **33,** 127 (1977).
36. J. Emsley, "The Elements," 2nd ed. Clarendon Press, Oxford, 1991.
37. W. Biltz, "Raumchemie der festen Stoffe." Verlag von Leopold Voss, Leipzig, 1934.
38. I. D. Brown and D. Altermatt, *Acta Crystallogr. Sect. B* **41,** 244 (1985).
39. The difference in energy zeros is completely irrelevant for such calculations since Bloch's theorem was used. Upon assuming cyclic boundary conditions, there is no contact to the vacuum level.
40. Note, however, that a perfect coincidence between the values from the one-electron and the many-electron theory can never be expected. The 0.001 eV precision of the H_{ii} and C values in Table 5 only intends to allow for future comparisons within the semiempirical and the *ab initio* schemes.
41. The ICOOP value of Cd^{2+}–Br^- bonding is much higher (0.282) and reflects the octahedron's shortened bond lengths compared to the prism, thus determining the size of the underlying overlap integral.